Int. J. Therm. Sci. (2000) 39, 697–708

S1290-0729(00)00229-5/FLA

Modification of molecular interactions at the interface crystal/heat transfer surface to minimize heat exchanger fouling

Markus Förster, Matthias Bohnet *

Institut für Verfahrens- und Kerntechnik, Langer Kamp 7, 38106 Braunschweig, Germany

(Received 3 September 1999, accepted 1 December 1999)

Abstract — Recent studies with respect to mitigate heat exchanger fouling spend only minor attention to the possibility of modifying molecular interactions at the interface between heat transfer surface (substrate) and adjacent crystalline deposit (adhesive). New anti-fouling strategies deal with a defined modification of these interactions to reduce the corresponding adhesive strength favouring the removal process due to the wall shear stress. By means of drop shape analysis the interfacial free energy adhesive/substrate has been determined. On the basis of numerous fouling experiments the interfacial defect model has been identified to serve as a tool to estimate the optimal choice of surface material. For the description of the influence of interfacial energies between two materials on adhesion both van der Waals and hydrophobic interactions making allowance for the presence of polar media have been analyzed. The geometric and harmonic mean approach (van der Waals forces only) is chosen for the description of metallic surfaces. For polymeric materials where repulsive interactions have to be taken into account, the Lewis acid–base approach (also considering hydrophobic interactions) is favoured. © 2000 Éditions scientifiques et médicales Elsevier SAS

precipitation fouling / induction period / interfacial free energy / van der Waals forces / hydrophobic interactions / adhesion

Nomenclature

A	area	m^2
C	constant	
c	concentration	$kg \cdot m^{-3}$
G	Gibbs free energy	J
k	overall heat transfer coefficient	$W \cdot m^{-2} \cdot K^{-1}$
$\dot{m}$	mass flow rate per unit area	$kg \cdot m^{-2} \cdot s^{-1}$
p	pressure	Pa
R_f	fouling resistance	$m^2 \cdot K \cdot W^{-1}$
T	temperature	K
t	time	h
w	flow velocity	$m \cdot s^{-1}$

Greek symbols

γ_{ij}	interfacial free energy between two adjacent phases i and j	$N \cdot m^{-1}$
λ_{12}	spreading coefficient of adhesive 1 on substrate 2	$N \cdot m^{-1}$
θ	contact angle	degree
τ	wall shear stress	$N \cdot m^{-2}$
ζ	adhesive strength	$N \cdot m^{-2}$

Superscripts and subscripts

0	clean surface
1	adhesive phase
2	substrate phase
3	surrounding phase
AB	Lewis acid–base
d	deposition
dis	dispersive
f	fouling layer
ind	induction period
LW	Lifshitz–van der Waals
pol	polar
r	removal
s	solid
v	vapour
w	wall
$\sim$	test liquid
$+$	electron acceptor
$-$	electron donor

* Correspondence and reprints.
m.bohnet@tu-bs.de

Abbreviations

CCD	charge coupled device
CVD	chemical vapour deposition
DLC	diamond like carbon
DLVO	named after Derjaguin, Landau, Verwey and Overbeek [8, 9]
DSA	drop shape analysis
FEP	fluorinated ethylene propylene
PFA	perfluoroalkoxy copolymer
PMMA	polymethylmethacrylate
PTFE	polytetrafluor ethylene

1. INTRODUCTION

The growth of fouling layers on heat transfer surfaces is a severe problem for industry [1–4]. Due to insulation these crystalline deposits contribute to the overall heat transfer coefficient deteriorating the performance of heat exchangers considerably. The decreased efficiency of heat transfer units can be desribed by the fouling resistance, i.e. the additional heat transfer resistance due to the fouling layer:

$$R_f = \frac{1}{k_f} - \frac{1}{k_0} \tag{1}$$

Here, k_f denotes the overall heat transfer coefficient for the fouled and k_0 for the clean surface, respectively. The fouling process can be divided into two periods, i.e. induction and fouling period. In the induction period the formation of stable nuclei at the heat transfer surface and the crystal growth take place. In the succeeding fouling period an increase of fouling resistance versus time can be measured due to the initiated formation of a compact fouling layer. *Figure 1* shows the texture of a crystalline $CaSO_4$-deposit at the beginning of the fouling period.

Both induction and fouling period consist of a deposition and removal process described by the deposition mass rate $\dot{m}_d$ and removal mass rate $\dot{m}_r$, respectively. The deposition mechanism of the fouling period depends on diffusion of the salt ions from the bulk to the solid fouling layer and a chemical reaction when the ions arrange themselves into the crystal lattice. The removal mechanism of the fouling period is mainly influenced by the interaction between wall shear stress due to the liquid flow and shear strength of the scaling. On the other hand, the deposition mechanism of the induction period is a function of the nucleation rate, whereas the removal mechanism is mainly affected by the adhesion between crystals and heat transfer surface as described in *figure 2*. A more

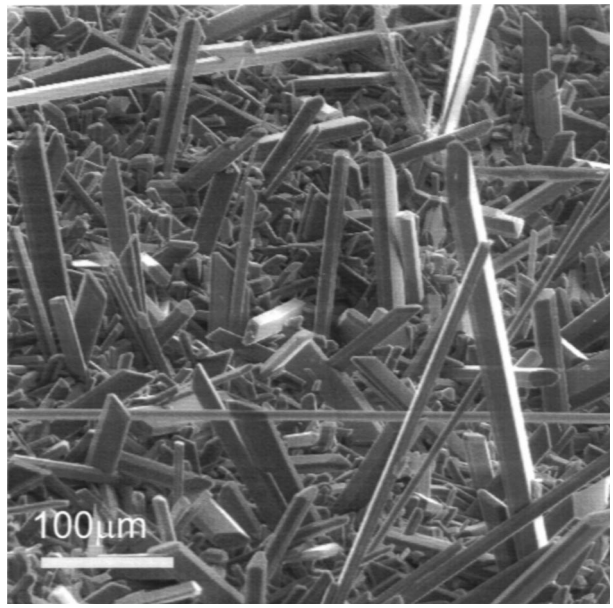

Figure 1. Texture of a fouling layer ($CaSO_4$) at the beginning of the fouling period.

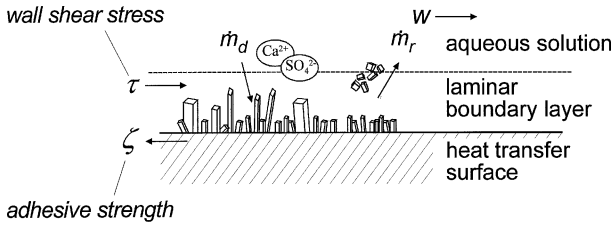

Figure 2. Deposition and removal during the induction period.

detailed description of the transport mechanisms can be found in [5, 6].

Modern anti-fouling strategies are based on approaches increasing the duration of the induction period and, hence, decreasing the adhesive strength between crystals and heat transfer surface. In order to relate physical properties of the interface crystal/heat transfer surface to adhesion the interfacial interactions have to be analyzed. *Figure 3* gives an overview of interactions playing a decisive role in adhesion. Oliveira [7] provides a detailed description of all relevant interactions.

In the succeeding sections approaches according to the DLVO theory (named after Derjaguin, Landau, Verwey and Overbeek [8, 9]) are discussed based on the assumption that dispersive and polar Lifshitz–van der Waals forces are of major importance for the adhesion mechanism. In addition, the commonly repulsive double layer forces due to the tendency of particular materials

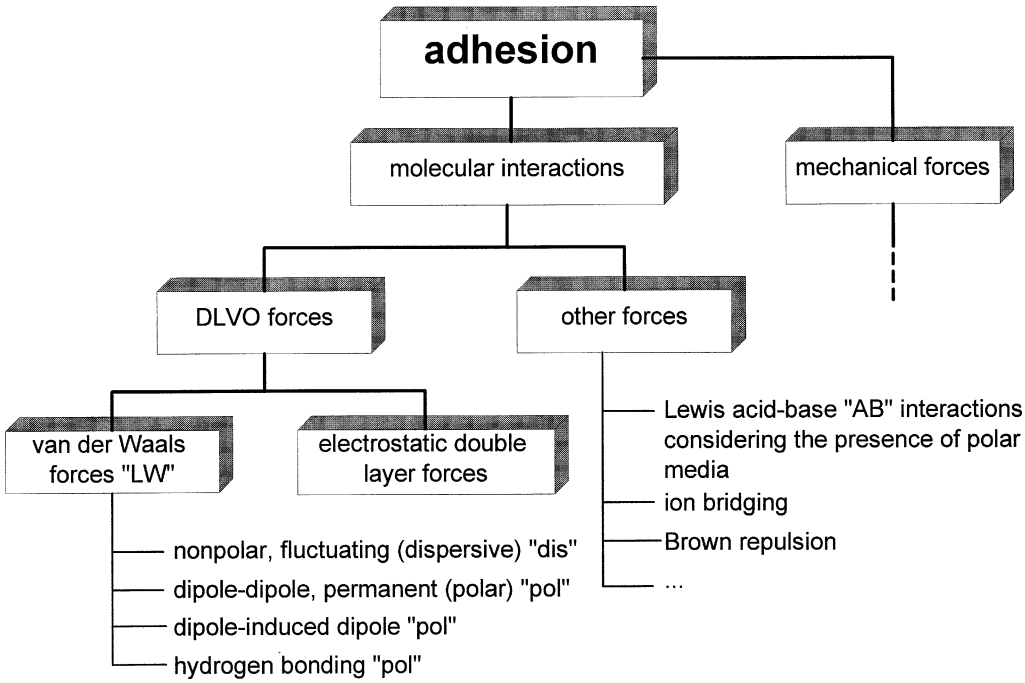

Figure 3. Interfacial interactions influencing adhesion.

to acquire an electrical charge when immersed in polar media are taken into account in order to explain the measured dependence of energy related interfacial properties of DLC coatings on fouling behaviour. According to van Oss [10] Lewis acid–base interactions in polar media (e.g., water) can cause anomalies in the theoretical interpretation of interfacial interactions using the DLVO theory. In contradiction to the latter theory considering attractive forces only, for some materials repulsive electron donor–electron acceptor interactions based on the Lewis acid–base theory can develop when the substrates are immersed in polar media. Therefore, the approach of van Oss is analyzed with respect to its ability to describe the influence of interfacial energies on adhesion.

2. FOULING EXPERIMENTS

In order to evaluate the dependence of interfacial characteristics at the interface crystal/heat transfer surface on adhesion during the induction period several surface materials have been exposed to the liquid flow of an aqueous calcium sulphate solution. The arrangement of the deployed measurement unit is given in *figure 4*.

In the storage tank the salt concentration of the aqueous calcium sulphate solution is controlled by conductimetry. A centrifugal pump realizes a continuous loop of the liquid flow. The filter avoids sedimentation of particles and secondary nucleation in the test sections since seed particles can influence nucleation behaviour considerably. The heat exchanger guarantees a constant inlet temperature at the test sections. Both second and third test section consist of annular test tubes for reference measurements. According to *figure 5*, for the first test section, a rectangular geometry has been chosen. The section includes a plate heat exchanger suited for a comfortable replacement of its heat transfer surface when different materials have to be characterized with respect to their fouling performance. The surface is electrically heated by three rod heaters. The temperature of the test surface is measured by six thermocouples in order to determine the fouling resistance. The wall of the test section contains a transparent section made of PMMA for the observation of the fouling process, especially of the induction period. This helps to identify regions which are preferred for nucleation.

Figures 6 and *7* provide the measured dependence of the fouling resistance R_f on time for metallic and polymeric surface materials. All test runs have been performed using an aqueous $CaSO_4$-solution of inverse solu-

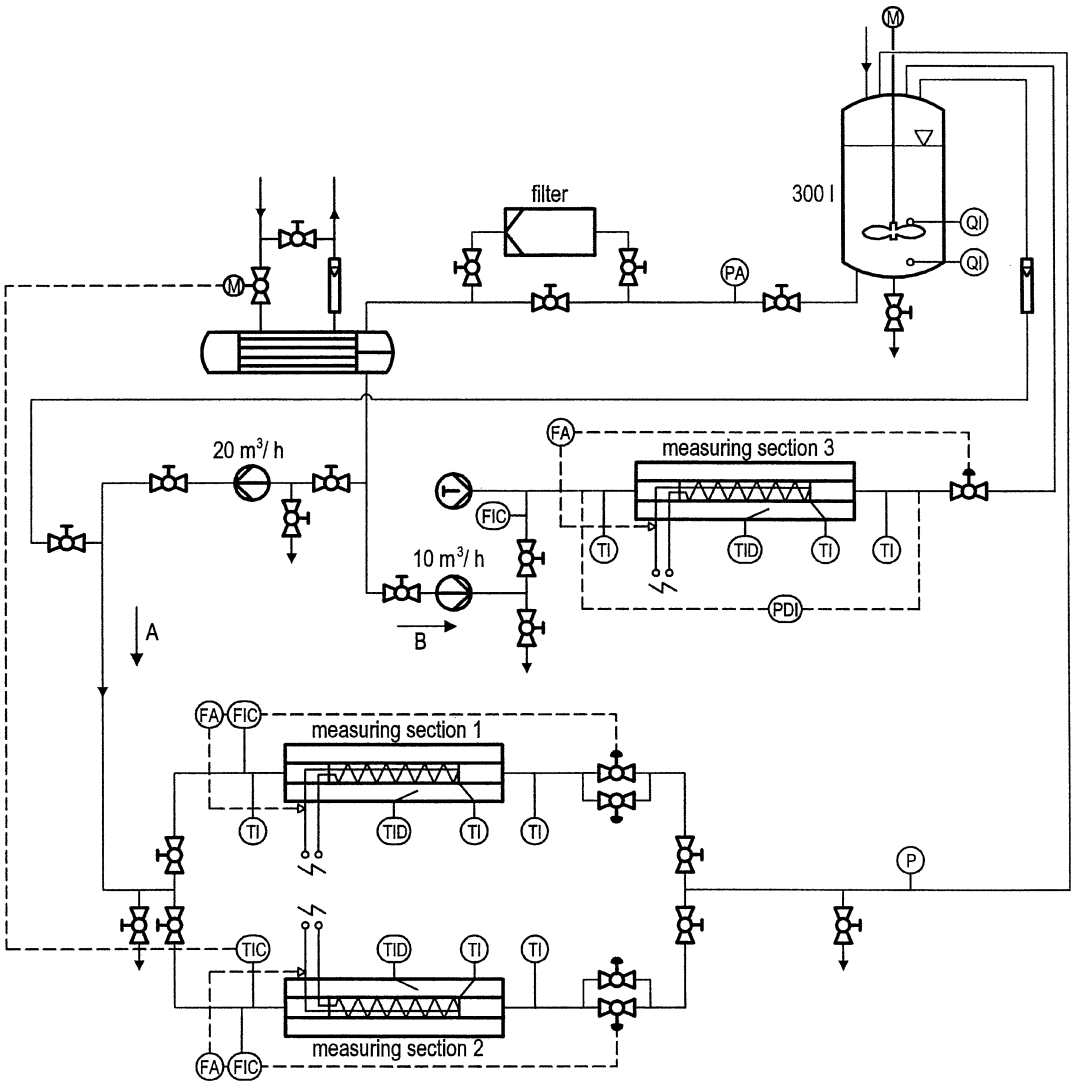

Figure 4. Experimental arrangement.

bility. The constant heat flux density is $\dot{q} = 31.8\ \mathrm{kW \cdot m^{-2}}$ giving an initial wall temperature of $T_{\mathrm{w},t=0} = 75\ ^{\circ}\mathrm{C}$. Due to a constant heat flow $T_{\mathrm{w},t=0}$ is equal to T_{f} defined as the temperature at the interface between fouling layer and heat transfer surface. Since T_{f} is less than the temperature of ebullition, only convective heat transfer has to be regarded.

In *figure 6* copper shows the most significant fouling tendency, whereas brass alloys, such as Ms(A) and Ms(B), correspond to longer induction periods compared to a common surface made of stainless steel. The deployment of new surface materials such as DLC coatings produced in a CVD process proved to be a strategy to increase the duration of the induction period. After more than 475 h the system is still within the induction period. The height of single crystals exceeds the thickness of the laminar boundary layer resulting in an increased turbulence which leads to an improved heat transfer and, hence, to negative values of R_{f}.

The fouling curves of PTFE, FEP and PFA coated surface materials given in *figure 7* contradict the widespread thesis that, as a consequence, the use of such "low energy" materials leads to long induction periods. In spite of having the lowest surface energy, *figure 7* shows a

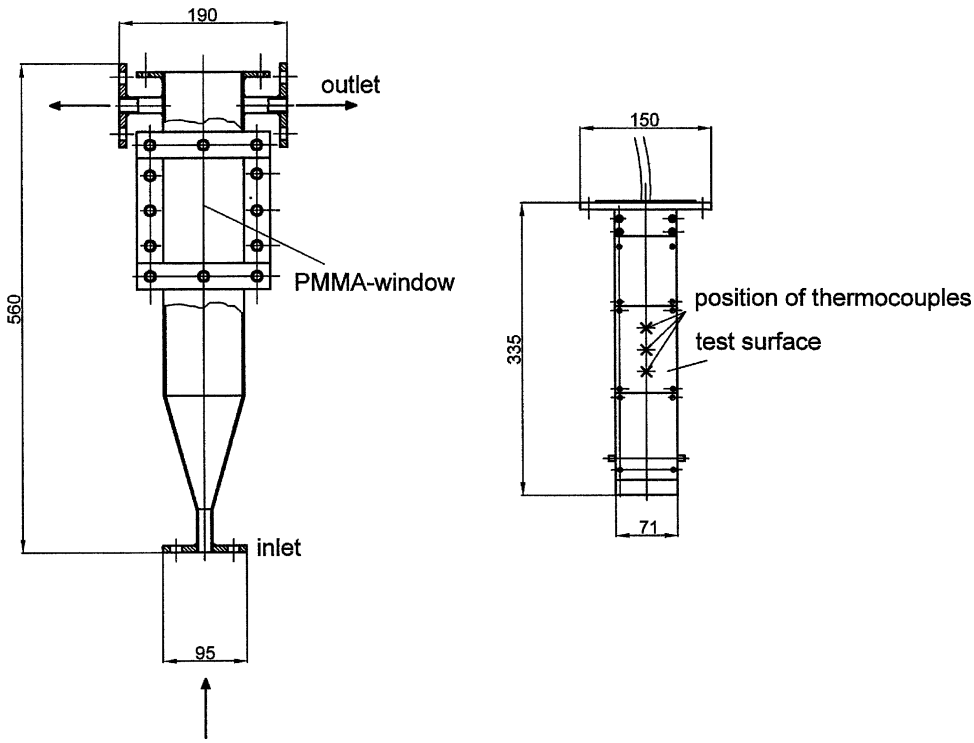

Figure 5. Plate heat exchanger.

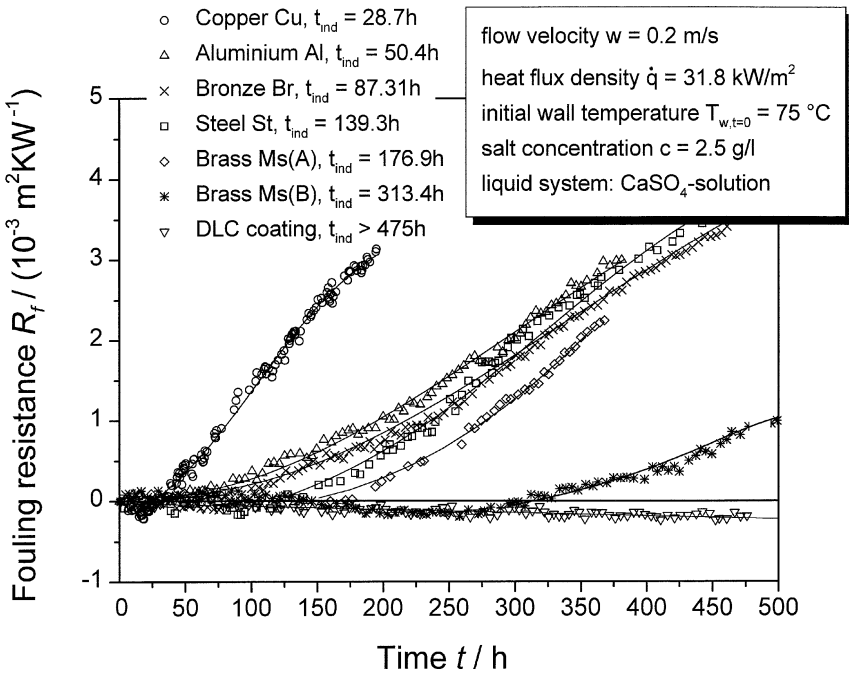

Figure 6. Fouling resistance versus time for metallic heat transfer surfaces.

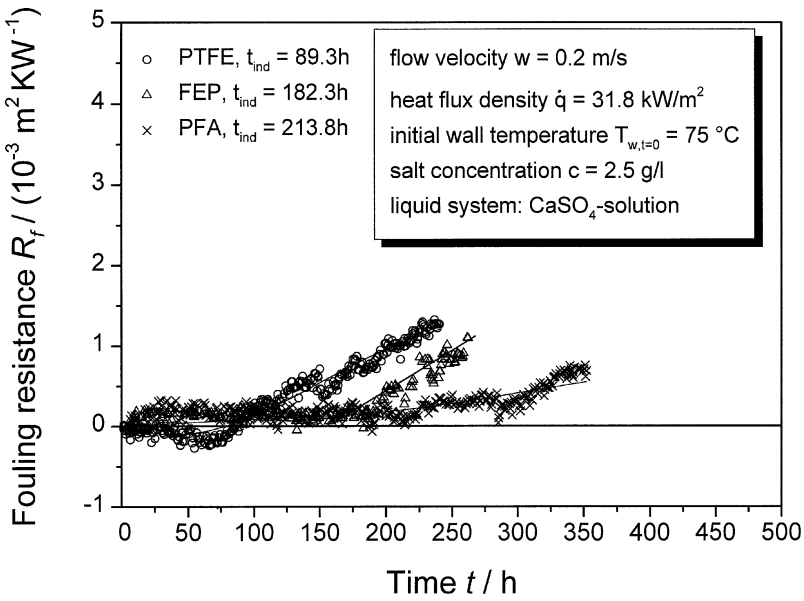

Figure 7. Fouling resistance versus time for polymeric heat transfer surfaces.

significant fouling tendency for PTFE. The deployment of polymeric coatings on common heat transfer surfaces made of stainless steel demands a minimal layer thickness resulting in an inhomogeneous texture of the surface coating due to the production process. The nonhomogeneity of surface material favours nucleation decreasing the duration of the induction period. Once a compact fouling layer has established under a constant heat flux, the polymeric material is destroyed because of its low temperature stability. Thus, the use of polymeric heat transfer surfaces is not suitable for heat exchangers for the operating conditions which have been examined.

For the investigation of low energy surfaces see also Müller-Steinhagen and Zhao [11].

3. INTERFACIAL MOLECULAR INTERACTIONS

3.1. Fundamentals

In order to evaluate the dependence of fouling behaviour on surface characteristics during the induction period, the physical mechanisms taking place at the interface crystal/heat transfer surface have to be analyzed. An important parameter influencing interfacial interactions is

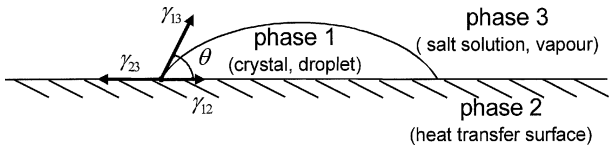

Figure 8. Interfacial free energies at the boundaries between three phases.

the interfacial free energy

$$\gamma_{ij} = \left(\frac{\partial G}{\partial A}\right)_{T,p} \tag{2}$$

defined as the total reversible work to create an interfacial area at the interface of the phases i and j [12]. Here, G denotes the Gibbs free energy of the system, T the temperature and p the pressure. If the adjacent phase j is vapour or vacuum γ_{ij} is also called "surface free energy" of phase i. In the following sections interfacial interactions are treated on the basis of an equilibrium of three phases in contact according to *figure 8*.

Here, a spherical adhesive (phase 1) is resting on a substrate (phase 2) in a surrounding phase (phase 3). For the treatment of equilibria the notation used is specified in *table I*. The state of aggregation of the adjacent phases depends on the field of application, that means, whether surface energies have to be determined by wetting experiments, or fouling layers on heat transfer surfaces in a surrounding liquid salt solution are regarded.

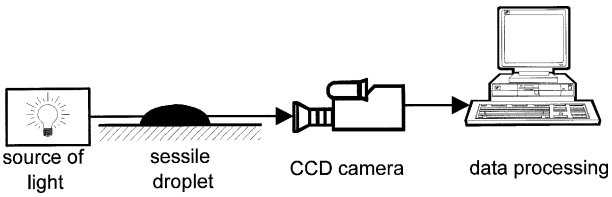

Figure 9. Experimental arrangement of the DSA measurement device.

TABLE I
Designation of phases.

Index	Wetting experiments	Fouling experiments	Designation of phase
1	droplet (“∼”)	crystal	adhesive
2	heat transfer surface	heat transfer surface	substrate
3	vapour	salt solution	surrounding phase

Resolving the interfacial free energies given in *figure 8* in a horizontal direction leads to the Young equation

$$\gamma_{23} = \gamma_{12} + \gamma_{13}\cos\theta \tag{3}$$

Since the surface free energy of the heat transfer surface influences the adhesion mechanism, γ_{23} is determined by means of a DSA measurement technique described in *figure 9*.

Here, a droplet of a test liquid is placed upon the surface to be characterized. By means of a CCD camera and a data processing system the image of the liquid droplet is digitized. Afterwards, the contour of the droplet is analyzed with respect to the determination of θ, the contact angle corresponding to the wetting equilibrium. The method demands that the physical properties of the test liquids are known. Different approaches to substitute γ_{12} in equation (3) are given in the succeeding sections.

3.2. Geometric and harmonic mean approach

In contrast with the approach chosen by Hamaker [13] who treats single interatomic interactions, Lifshitz follows a macroscopic approach to describe interfacial interactions considering nonpolar and polar interactions found by van der Waals [10]. According to Fowkes [14] the interfacial energy can be divided into a dispersive (index “dis”) and a polar (index “pol”) component assumed that van der Waals forces (*figure 3*) are predominant.

Owens and Wendt [15] suggest a geometric mean approach to calculate γ_{12} which is mainly applied for nonpolar systems where the ionization potential of adhesive and substrate equals each other, i.e.

$$\gamma_{12} = \gamma_{13} + \gamma_{23} - 2\left(\sqrt{\gamma_{13}^{\mathrm{dis}}\gamma_{23}^{\mathrm{dis}}} + \sqrt{\gamma_{13}^{\mathrm{pol}}\gamma_{23}^{\mathrm{pol}}}\right) \tag{4}$$

For the characterization of low energy systems such as polymers or organic liquids Wu [12] favours a harmonic mean approach based on the assumption that the polarizabilities of adhesive and substrate are similar:

$$\gamma_{12} = \gamma_{13} + \gamma_{23} - 4\left(\frac{\gamma_{13}^{\mathrm{dis}}\gamma_{23}^{\mathrm{dis}}}{\gamma_{13}^{\mathrm{dis}} + \gamma_{23}^{\mathrm{dis}}} + \frac{\gamma_{13}^{\mathrm{pol}}\gamma_{23}^{\mathrm{pol}}}{\gamma_{13}^{\mathrm{pol}} + \gamma_{23}^{\mathrm{pol}}}\right) \tag{5}$$

Since the heat transfer surfaces to be characterized concerning fouling performance and surface energy include nonpolar as well as low energy materials both the geometric and harmonic mean approach are deployed to determine interfacial energies. Either equation (4) or (5) can be used to substitute the unknown interfacial energy γ_{12} in the Young equation (3). In order to determine the surface free energy γ_{23} of the heat transfer surface as well as dispersive and polar components, the physical properties of the test liquids are required. An increasing amount of test liquids increases the accuracy of the wetting experiments. According to *table II*, six test liquids are deployed. Furthermore, a comparison between measured and literature data of the absolute surface free energy $\widetilde{\gamma}_{13}$ is provided. Here, “∼” is used to distinguish between interfacial energies corresponding to droplets and crystals. A detailed designation of the phases is presented in *table I*. Since measurement is in good agreement with literature data for $\widetilde{\gamma}_{13}$, $\widetilde{\gamma}_{13}^{\mathrm{dis}}$ and $\widetilde{\gamma}_{13}^{\mathrm{pol}}$ given in *table II* can be utilized.

Having measured the contact angle between test liquid and heat transfer surface the only remaining unknowns in equation (3) are $\gamma_{23}^{\mathrm{dis}}$ and $\gamma_{23}^{\mathrm{pol}}$ since the absolute free energy γ_{23} can be derived according to Fowkes [14]:

$$\gamma_{ij} = \gamma_{ij}^{\mathrm{dis}} + \gamma_{ij}^{\mathrm{pol}} \tag{6}$$

Hence, at least two liquids are needed to determine γ_{23}, $\gamma_{23}^{\mathrm{dis}}$ and $\gamma_{23}^{\mathrm{pol}}$. Before accurate DSA measurements can be performed, a careful cleaning process has to be carried out in order to minimize surface contamination. The following cleaning stages have been chosen according to Junghahn [17]: (1) soap water; (2) methyl alcohol;

TABLE II
Physical properties of the test liquids.

Test liquid	$\widetilde{\gamma}_{13}$ (mN·m^{-1}) measured	$\widetilde{\gamma}_{13}$ (mN·m^{-1}) [14]	$\widetilde{\gamma}_{13}^{dis}$ (mN·m^{-1}) [14]	$\widetilde{\gamma}_{13}^{pol}$ (mN·m^{-1}) [14]	ρ (kg·m^{-3})
Water	72.80	72.80	21.80	51.00	998
Ethylene glycol	48.10	48.20	18.91	29.29	1113
Formamide	58.30	58.20	39.50	18.70	1132
1-Bromnaphthalene	44.30	44.60	41.20	3.40	1488
Methylene iodide	51.00	50.80	48.50	2.30	3318
Glycerin	64.00	63.30	20.22	43.08	1260

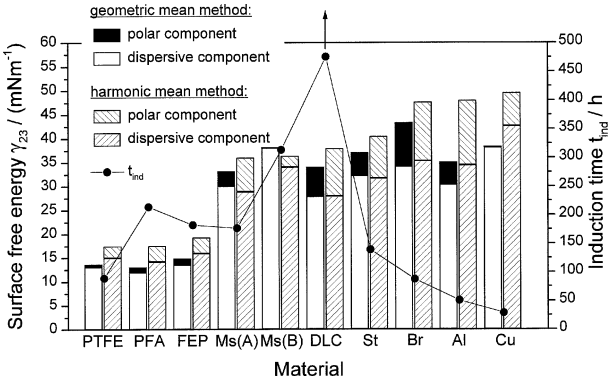

Figure 10. Surface energy characteristics and induction time (geometric and harmonic mean approach).

(3) ethanol; (4) destilled water; (5) acetone; (6) destilled water; (7) drying stove.

Figure 10 shows results of wetting experiments on heat transfer surfaces. In addition, the measured induction time t_{ind} is given. For the DLC coating, t_{ind} have to be extrapolated in the direction of the ordinate because no increase in fouling resistance versus time could be detected after 475 h.

The comparison of surface energy data with induction time yields no correlation between interfacial interaction heat transfer surface/vapour and fouling behaviour. Thus, the choice of surface material with respect to least fouling occurence cannot be based on surface properties of the particular heat transfer surface only. In order to find the optimal surface material the adjacent crystalline deposit has to be taken into account since the latter phase also influences molecular interaction at the interface crystal/heat transfer surface. So far, it is rather complicated to measure realistic surface properties of single crystals making allowance for their texture. Furthermore, no useful literature data can be found to solve this problem. As a first approach it is assumed that the energy related surface properties of the adhesive side of a fouling layer (*figure 11*) may be used for the description of adhesion of crystals and crystalline clusters during the induction period.

Figure 11. Adhesive side of a fouling layer.

TABLE III
Surface energy characteristics of the adhesive side of a fouling layer.

γ_{13}^{dis} (mN·m^{-1})	γ_{13}^{pol} (mN·m^{-1})	γ_{13} (mN·m^{-1})
36.51[a]	7.40[a]	43.91[a]
37.68[b]	10.20[b]	47.88[b]

[a] Referred to geometric mean approach.
[b] Referred to harmonic mean approach.

The adhesive side of a fouling layer has been examined by means of the DSA measurement unit to gain information of γ_{13}, γ_{13}^{dis} and γ_{13}^{pol} (*table III*) now corresponding to "fouling experiments" according to *table I*.

Since the surface energy properties of both crystalline deposit (adhesive) and heat transfer surface (substrate) are accessible using the DSA measurement technique the interfacial free energy γ_{12} adhesive/substrate can be

derived by means of equation (4) or (5). This enables one to determine the spreading coefficient λ_{12} defined in equation (7)

$$\lambda_{12} = \gamma_{23} - \gamma_{13} - \gamma_{12} \tag{7}$$

For various polymer pairs the interfacial defect model is capable of relating wetting characteristics to the adhesive strength ζ given that van der Waals interactions are predominant [12], according to

$$\zeta = C\left(1 - \frac{\lambda_{12}}{\gamma_{23}}\right)^{-1} \tag{8}$$

C refers to the mechanical properties of the system such as the Young's modulus. Increasing λ_{12} is accompanied by an improved wettability and, as a consequence, by an increase of ζ due to less interfacial defects and contact area, respectively. Two special cases have to be considered:

(i) The equilibrium of forces according to the Young equation (3) is valid which means $0° \leq \theta \leq 180°$. With the help of equations (3) and (7) the spreading coefficient may be evaluated from

$$\lambda_{12} = \gamma_{13}(\cos\theta - 1) \tag{9}$$

If no spreading occurs corresponding to $\theta = 180°$, equation (9) yields $\lambda_{12} = -2\gamma_{13}$. In the case of spontaneous spreading, i.e. $\theta = 0°$, equation (9) gives $\lambda_{12} = 0$.

(ii) For $\lambda_{12} > 0$ equation (3) cannot be taken since the system is not in the state of equilibrium any longer.

Combining equations (7) and (8) yields

$$\zeta = C\left(1 + \frac{\lambda_{12}}{\gamma_{13} + \gamma_{12}}\right) \tag{10}$$

Hence, maximum wettability is a premise for maximum adhesion according to

$$\lambda_{12} \overset{!}{\rightarrow} \infty \quad \text{(condition for optimum adhesion)} \tag{11}$$

Since dispersive and polar van der Waals forces are assumed to be of major importance for precipitation fouling [6], the compatibility of the interfacial defect model with the fouling phenomenon has been evaluated. In *figure 12* wetting characteristics described by λ_{12} are opposed to fouling behaviour characterized by the induction time t_{ind}.

The results accumulated in *figure 12* verify the capability of the interfacial defect model to describe the functional dependence of fouling behaviour on wettability for metallic heat transfer surfaces since a high value of

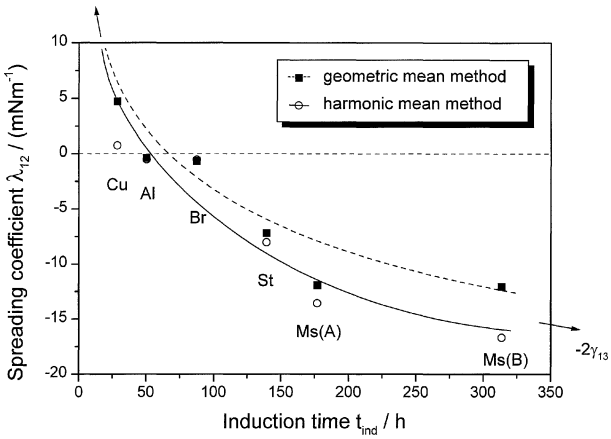

Figure 12. Spreading coefficient versus induction time for metallic heat transfer surfaces (geometric and harmonic mean approach).

TABLE IV
Wetting and fouling characteristics of DLC and polymeric surface materials.

Surface material	λ_{12} (mN·m^{-1})	t_{ind} (h)
PTFE	-39.97^a, -44.87^b	89.3
FEP	-37.03^a, -40.88^b	182.3
PFA	-40.30^a, -44.49^b	213.8
DLC	-10.52^a, -11.38^b	>475

[a] Referred to geometric mean approach.
[b] Referred to harmonic mean approach.

λ_{12} corresponds to a high adhesive strength crystal/heat transfer surface resulting in a short duration of the induction period. By means of the interfacial defect model the fouling performance of particular materials can be predicted on the basis of DSA measurements only. The surface material with respect to a long induction time should lead to low spreading coefficients. The condition for least fouling occurence can be stated according to

$$\lambda_{12} \overset{!}{\rightarrow} -2\gamma_{13} \quad \text{(condition for least fouling occurence)} \tag{12}$$

On the other hand, the description of interfacial interaction by means of the previously introduced model fails for polymeric surface materials and DLC coatings. None of the (t_{ind}/λ_{12}) data points according to *table IV* fit to the regression curve provided in *figure 12*.

The discrepancy between model and reality can be explained by means of an approach based on the Lewis acid–base theory.

3.3. Lewis acid–base approach

According to van Oss [10] the problem with the use of geometric and harmonic means based only on van der Waals forces is that none of this treatments accounts for polar interactions due to the presence of polar media (e.g., water). These electron donor–electron acceptor interactions are explained using the Lewis acid–base theory. Van Oss suggests an equation to calculate the interfacial free energy γ_{ij} as a function of a Lifshitz–van der Waals component (index "LW") and a Lewis acid–base component (index "AB") by

$$\gamma_{ij} = \gamma_{ij}^{\mathrm{LW}} + \gamma_{ij}^{\mathrm{AB}} \tag{13}$$

where the "AB" component comprises an electron acceptor (index "+") and an electron donor (index "−") parameter, i.e.

$$\gamma_{ij}^{\mathrm{AB}} = 2\sqrt{\gamma_{ij}^{+}\gamma_{ij}^{-}} \tag{14}$$

Analogous to the preceding methods of Owens and Wu the Young equation (3) is deployed to determine energy related characteristics of heat transfer surfaces by DSA measurements. The unknown interfacial energy γ_{12} is substituted by

$$\gamma_{12} = \left(\sqrt{\gamma_{13}^{\mathrm{LW}}} - \sqrt{\gamma_{23}^{\mathrm{LW}}}\right)^2 + 2\left(\sqrt{\gamma_{13}^{+}\gamma_{13}^{-}} + \sqrt{\gamma_{23}^{+}\gamma_{23}^{-}} - \sqrt{\gamma_{13}^{+}\gamma_{23}^{-}} - \sqrt{\gamma_{13}^{-}\gamma_{23}^{+}}\right) \tag{15}$$

The approaches of Owens and Wu according to equations (4) and (5) to substitute γ_{12} in the Young equation (3) cannot describe forces otherwise but attractive refering to positive values of γ_{12}. In contrast, equation (15) suggested by van Oss enables one to calculate both positive and negative values of γ_{12} corresponding to attractive and repulsive interactions, respectively. Applying equations (3) and (13)–(15), values of $\widetilde{\gamma}_{13}^{\mathrm{LW}}$, $\widetilde{\gamma}_{13}^{+}$ and $\widetilde{\gamma}_{13}^{-}$ given in *table V* as well as contact angles derived by the DSA measurement technique, there are still three unknown parameters $\gamma_{23}^{\mathrm{LW}}$, γ_{23}^{+} and γ_{23}^{-}, describing the energy properties of the substrate. DSA measurements with three test liquids are sufficient to solve the system of equations.

In *figure 13* the measured energy related properties based on the Lewis acid–base theory are accumulated for various materials including a fouling layer as well as calcium sulphate hemihydrate and dihydrate deposits. Nearly all materials which have been examined manifest only a γ_{13}^{-} parameter. According to equation (14) the $\gamma_{13}^{\mathrm{AB}}$ component of the total surface free energy equals zero. However, such substances which are designated as "monopolar" can strongly interact with bipolar materials, and with monopolar materials of the opposite polarity.

TABLE V
Physical properties of test liquids [7].

Test liquid	$\widetilde{\gamma}_{13}^{\mathrm{LW}}$ (mN·m^{-1})	$\widetilde{\gamma}_{13}^{\mathrm{AB}}$ (mN·m^{-1})	$\widetilde{\gamma}_{13}^{+}$ (mN·m^{-1})	$\widetilde{\gamma}_{13}^{-}$ (mN·m^{-1})
Water	21.8	51.0	25.5	25.5
Formamide	39.0	19.1	2.3	39.6
Methylene iodide	50.8	0	0	0

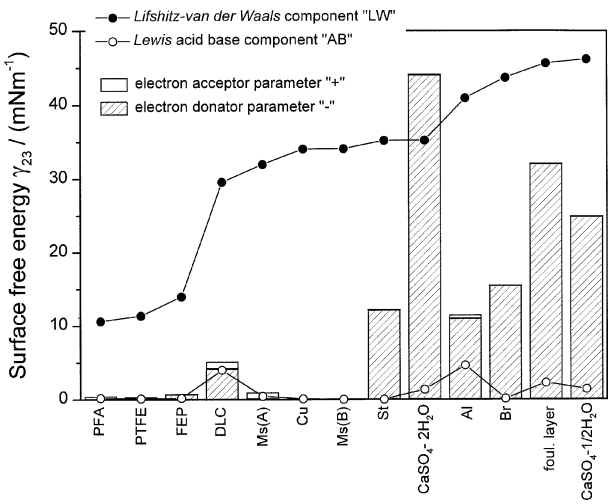

Figure 13. Energy related properties of various materials (Lewis acid–base approach).

Calcium sulphate hemihydrate $CaSO_4{-}\frac{1}{2}H_2O$ and dihydrate $CaSO_4{-}2H_2O$ defined modifications of gypsum, serving as the salt phase in fouling experiments, have been examined with respect to wetting characteristics by means of the Washburn method [18]. This method is especially suited for porous materials. Using the Dupré equation [19] the interaction energy (index "132") between crystal "1" and heat transfer surface "2" immersed in a liquid "3" may be described as

$$\begin{aligned}\Delta G_{132} &= \Delta G_{132}^{\mathrm{LW}} + \Delta G_{132}^{\mathrm{AB}} \\ &= 2\Big[\sqrt{\gamma_{1\mathrm{v}}^{\mathrm{LW}}\gamma_{3\mathrm{v}}^{\mathrm{LW}}} + \sqrt{\gamma_{2\mathrm{v}}^{\mathrm{LW}}\gamma_{3\mathrm{v}}^{\mathrm{LW}}} - \sqrt{\gamma_{1\mathrm{v}}^{\mathrm{LW}}\gamma_{2\mathrm{v}}^{\mathrm{LW}}} \\ &\quad - \gamma_{3\mathrm{v}}^{\mathrm{LW}} + \sqrt{\gamma_{3\mathrm{v}}^{+}}\left(\sqrt{\gamma_{1\mathrm{v}}^{-}} + \sqrt{\gamma_{2\mathrm{v}}^{-}} - \sqrt{\gamma_{3\mathrm{v}}^{-}}\right) \\ &\quad + \sqrt{\gamma_{3\mathrm{v}}^{-}}\left(\sqrt{\gamma_{1\mathrm{v}}^{+}} + \sqrt{\gamma_{2\mathrm{v}}^{+}} - \sqrt{\gamma_{3\mathrm{v}}^{+}}\right) \\ &\quad - \sqrt{\gamma_{1\mathrm{v}}^{+}\gamma_{2\mathrm{v}}^{-}} - \sqrt{\gamma_{1\mathrm{v}}^{-}\gamma_{2\mathrm{v}}^{+}}\Big]\end{aligned} \tag{16}$$

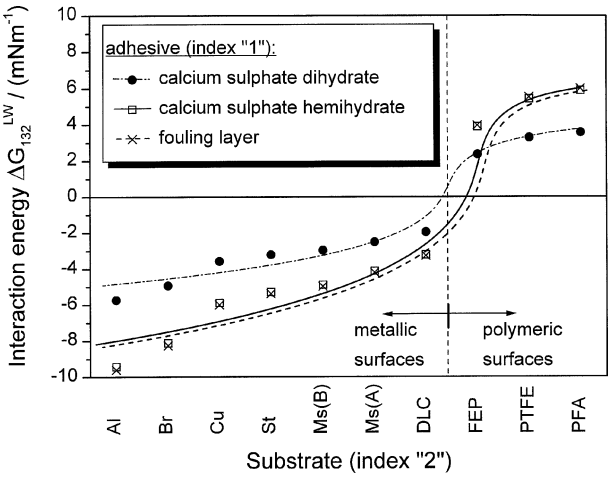

Figure 14. Interaction energy $\Delta G_{132}^{\mathrm{LW}}$ as a function of the system adhesive/substrate.

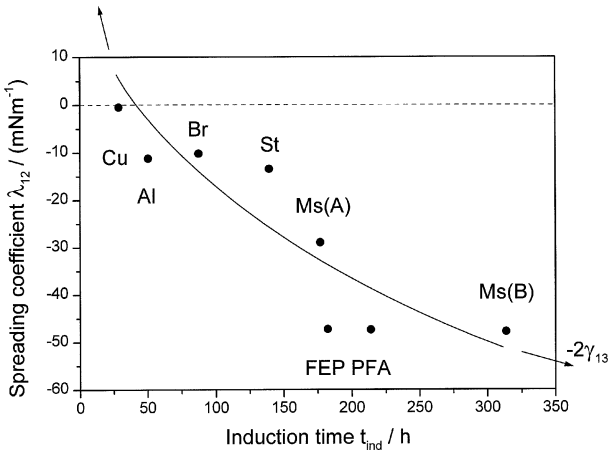

Figure 15. Spreading coefficient versus induction time (Lewis acid–base approach).

$\gamma_{i\mathrm{v}}$ denotes the interfacial free energy between phase i and vapour derived by the DSA measurement technique. For the treatment of the fouling phenomenon it is assumed that the physical properties of the surrounding phase are close to those of water. Thus, values of $\gamma_{3\mathrm{v}}^{\mathrm{LW}} = \widetilde{\gamma}_{13}^{\mathrm{LW}}$ and $\gamma_{3\mathrm{v}}^{\mathrm{AB}} = \widetilde{\gamma}_{13}^{\mathrm{AB}}$ given in *table V* can be deployed. Negative values of ΔG_{132} correspond to attractive forces whereas positive values appear when repulsive interactions between adhesive and substrate are predominat. In *figure 14* the Lifshitz–van der Waals component of ΔG_{132} is presented as a function of the surface material of the substrate. In the diagram three curves can be found according to three different adhesives: $CaSO_4$–$2H_2O$, $CaSO_4$–$\frac{1}{2}H_2O$ and a fouling layer.

From *figure 14* the conclusion can be drawn that the constitution of the crystal lattice of the adhesive side of the fouling layer is close to calcium sulphate hemihydrate since the corresponding interaction energies resemble each other. In contrast to metallic surfaces, for polymeric surface materials positive values of $\Delta G_{132}^{\mathrm{LW}}$ can be determined indicating that repulsive Lifshitz–van der Waals forces are active. Because repulsion can never be taken into account by the geometric or harmonic mean method the Lewis acid–base approach has to be favoured between materials which tend to have high positive values of the interfacial energy when immersed in polar media. By means of equation (7) the spreading coefficient λ_{12} can be determined. In *figure 15* λ_{12} is presented as a function of the induction time t_{ind} including data of the polymers FEP and PFA.

The deviation of the corresponding data points from the regression curve can be explained taking also geometric surface properties into account. By means of a surface texture measuring unit it was confirmed that the surface topographies of the metallic heat transfer surfaces resemble each other. Due to the production process a polymeric surface tends to be more cleaved than metallic heat transfer surfaces. Therefore, PFA and FEP have more critical flaws which serve as regions for preferred nucleation reducing t_{ind}. A more detailed discussion of the influence of surface geometry can be found in [6].

The molecular interactions between DLC coated surface and fouling layer ($\lambda_{12} = -16.9$ mN·m^{-1}; $t_{\mathrm{ind}} > 475$ h) can be described neither by the geometric/harmonic mean methods nor by the Lewis acid–base theory because interfacial interactions such as electrostatic double layer forces are predominat.

As a conclusion, the wide-spread methods of Owens and Wu should be taken when the difference between geometric/harmonic mean and Lewis acid–base approach may not appear terribly important, i.e. when under the condition of monopolarity $\gamma_{12}^{\mathrm{AB}}$ remains zero and no severe repulsive interactions arise. For metallic surfaces, the geometric and harmonic mean methods should be favoured since they are still state of the art been used frequently in many research areas for the combination of wetting and adhesion. On the other hand, the Lewis acid–base approach has to be applied whenever the repulsive hydrophobic interactions become more significant as in the case of the polymeric surface materials which have been examined.

4. CONCLUSIONS AND FUTURE WORK

For the minimization of heat exchanger fouling the interfacial defect model has been analyzed with respect to its ability to identify the optimal choice of surface material. Besides dispersive and polar van der Waals forces at the interface crystal/heat transfer surface, also Lewis acid–base interactions have been taken into account.

Future research work should contribute to an even more detailed description of the influence of surface properties of heat exchangers on precipitation fouling, e.g., by a description of interfacial interactions considering double layer forces.

Then, also surface topography should be analyzed with respect to adhesion mechanisms since mechanical forces at the interface crystal/heat transfer surface are responsible for discrepancies between reality and theory which is described by current models on the basis of molecular interactions only. Here, the definition of an appropriate surface texture parameter would be helpful, being able to describe the influence of the depth and width of profile elements of surface contour on crystal attachement during the induction period.

Crystalline deposits can be exposed to an ageing process on the molecular level [20]. The presence of this process is suggested as another approach of fouling mitigation since the control of wall temperature could initiate a decrease of adhesive strength of the fouling layer due to dynamic phase transitions of the crystal lattice. The examination of the influence of the ageing process on molecular interactions at the interface fouling layer/heat exchanger is subject to current research work.

Acknowledgement

Financial support for this research work has been granted by the "Deutsche Forschungsgemeinschaft".

REFERENCES

[1] Augustin W., Bohnet M., Influence of the ratio of free hydrogen ions on crystallization fouling, Chem. Engrg. Process. 34 (1995) 79–85.

[2] Bohnet M., Fouling of heat transfer surfaces, Chem. Engrg. Technol. 10 (1987) 113–125.

[3] Bohnet M., Augustin W., Middis J., Effect of surface structure on fouling behaviour, in: Proceedings of the Eurotherm Seminar 23, Grenoble, 1992, pp. 39–46.

[4] Hirsch H., Scher- und Haftfestigkeit kristalliner Foulingschichten auf wärmeübertragenden Flächen, Shaker Verlag, Aachen, 1997.

[5] Förster M., Augustin W., Bohnet M., Verminderung des Kristallisationsfoulings in Wärmeübertragern, in: Beiträge zur Kristallisation anorganischer Stoffe aus Lösungen, Freiberger Forschungsheft A 853, TU Bergakademie Freiberg, 1999.

[6] Förster M., Augustin W., Bohnet M., Influence of the adhesion force crystal/heat exchanger surface on fouling mitigation, Chem. Engrg. Process. 38 (1999) 449–461.

[7] Oliveira R., Understanding adhesion: A means for preventing fouling, Experimental Thermal and Fluid Science 14 (1991) 319–322.

[8] Derjaguin B.V., Churaev N.V., Muller V.M., Surface Forces, Consultans Bureau, New York, 1987.

[9] Verwey E.J.W., Overbeek J.Th.G., Theory of Stability of Lyophobic Colloids, Elsevier, Amsterdam, 1948.

[10] Van Oss C.J., Interfacial Forces in Aqueous Media, Marcel Dekker, New York, 1994.

[11] Müller-Steinhagen H., Zhao Q., Investigation of low fouling surface alloys made by ion implantation technology, Chem. Engrg. Sci. 52 (1997) 3321–3332.

[12] Wu S., Polymer Interface and Adhesion, Marcel Dekker Inc., New York, 1982.

[13] Hamaker H.C., A general theory of lyophobic colloids, Physica 4 (1937) 1058.

[14] Fowkes F.M., Dispersion force contribution to surface and interfacial tensions, contact angles and heats of immersion, in: Advances in Chemistry Series 43, Am. Chem. Soc., Washington, 1964, pp. 99–111.

[15] Owens D.K., Wendt R.C., Estimation of surface energy, Journal of Applied Polymer Science 13 (1969) 1741–1747.

[16] Trojan K., Untersuchungen zum Einfluß netzwerkmodifizierender Elemente auf die freie Oberflächenenergie amorpher Kohlenwasserstoff-Schichten, VDI-Fortschrittsberichte 5 (1996) No. 431.

[17] Junghahn L., Untersuchungen über die Krustenbildung an metallischen Werkstoffen, Forschungsber. 927, Westdeutscher Verlag, 1960.

[18] Grundke K., Boerner M., Jacobasch H.-J., Characterization of fillers and fibres by wetting electrokinetic measurements, Colloids and Surfaces 58 (1991) 47–59.

[19] Dupré A., Théorie Mécanique de la Chaleur, Gauthier-Villars, Paris, 1869.

[20] Mullin J.W., Crystallization, Butterworth-Heinemann, Oxford, 1993.